


Ti_{0.8}O₂ Nanosheets Inhibit Lung Cancer Stem Cells by Inducing Production of Superoxide Anion

Nalinrat Petpiroon, Narumol Bhummaphan, Rapeepun Soonnarong, Wipa Chantarawong, Tosapol Maluangnont, Varisa Pongrakhananon, and  Pithi Chanvorachote

Department of Pharmacology and Physiology, Faculty of Pharmaceutical Sciences (N.P., W.C., V.P., P.C.), Interdisciplinary Program of Biomedical Sciences, Faculty of Graduate School (N.B.), Interdisciplinary Program of Pharmacology Graduate School (R.S.), and Cell-based Drug and Health Products Development Research Unit (N.P., N.B., R.S., W.C., V.P., P.C.), Chulalongkorn University, Bangkok, Thailand; and College of Nanotechnology, King Mongkut's Institute of Technology Ladkrabang, Bangkok, Thailand (T.M.)

Received September 13, 2018; accepted February 2, 2019

ABSTRACT

Recent research into the cancer stem cell (CSC) concept has driven progress in the understanding of cancer biology and has revealed promising CSC-specific targets for drug discovery efforts. As malignancies of lung cancer have been shown to be strongly associated with activities of CSCs, we examined the effects of Ti_{0.8}O₂ nanosheets on these cells. Here we show that the nanosheets target lung CSCs but not normal primary dermal papilla (DP) stem cells. Whereas Ti_{0.8}O₂ caused a dramatic apoptosis along with a decrease in CSC phenotypes, in primary human DP cells such effects of nanosheets have been minimal. Nanosheets reduced the ability of lung cancer cells to generate three-dimensional tumor spheroids, lung CSC markers (CD133 and ALDH1A1), and CSC transcription factors (Nanog and Oct-4). Ti_{0.8}O₂ nanosheets reduced CSC

signaling through mechanisms involving suppression of protein kinase B (AKT) and Notch-1 pathways. In addition, the nanosheets inhibited the migration and invasive activities of lung cancer cells and reduced epithelial-to-mesenchymal transition (EMT) markers as N-cadherin, vimentin, and Slug, as well as metastasis-related integrins (integrin- α v and integrin- β 1). Importantly, we found that the selectivity of the Ti_{0.8}O₂ nanosheets in targeting cancer cells was mediated by induction of cellular superoxide anion in cancerous but not normal cells. Inhibition of nanosheet-induced superoxide anion restored the suppression of CSC and EMT in cancer cells. These findings demonstrate a promising distinctive effect of Ti_{0.8}O₂ nanosheets on lung CSC that may lead to opportunities to use such a nanomaterial in cancer therapy.

Introduction

Lung cancer has been considered one of the leading life-threatening cancers for several years as its mortality rate is considerably high in comparison with other human cancers; deaths from lung cancer make up nearly 20% of cancer deaths worldwide (Ferlay et al., 2015). Advances in molecular biology as well as translational research have heralded important moves in the comprehension of lung cancer, in particular with regard to the more common non-small cell lung cancer (NSCLC) type, which accounts for 80% of lung cancers. The current therapeutic approaches—surgery, radiotherapy, chemotherapy, and targeted therapy—exhibit various outcomes depending on the cancer subtype and stage. In early stages, a

good response is observed in most cases; however, the long-term survival of late-stage patients is negatively impacted by disease relapse (Molina et al., 2008).

Accumulating knowledge has implicitly revealed that NSCLC is heterogeneous in nature with various molecular signatures underlying the hierarchy of cancer stem cell (CSCs) and non-CSC populations (Neelakantan et al., 2015). In general, CSC is a rare specific cancer cell arising in the tumor and referred to as “tumor-initiating cell.” CSCs have been identified in many solid tumors and have been shown to be a key player in cancer initiation, progression, and metastasis (Chen et al., 2013). Increasing evidence from different sources suggests that cells possessing CSC-like features are resistant to current chemotherapies, and their persistence leads to relapse of disease (Zhao, 2016). Therefore, novel therapeutic strategies targeting these cancer-initiating cells are now among the principle endeavors for the improvement of clinical outcomes.

This study was supported by the grant from the Ratchadaphisek Somphot Fund for Postdoctoral Fellowship, Chulalongkorn University, and a grant for International Research Integration: Chula Research Scholar, Ratchadaphisek Somphot Endowment Fund, Chulalongkorn University.
<https://doi.org/10.1124/mol.118.114447>.

ABBREVIATIONS: 2D, two-dimensional; AKT, protein kinase B; ALDH1A1, aldehyde dehydrogenase 1 family, member A1; AFM, atomic force microscopy; CD133, prominin-1; CSC, cancer stem cell; DCF, 2',7'-dichlorofluorescein; DHE, dihydroethidium; EMT, epithelial-to-mesenchymal transition; FBS, fetal bovine serum; GSK3 β , glycogen synthase kinase 3 beta; HPF, 3'-p-(hydroxyphenyl) fluorescein; MnTBAP, Mn(III)tetrakis (4-benzoic acid) porphyrin; MTT, 3-(4,5-dimethylthiazol-2-yl)-2,5-diphenyltetrazolium bromide; NSCLC, non-small cell lung carcinoma; PBS, phosphate-buffered saline; PI, propidium iodide; p-Oct-4, phosphorylation of octamer-binding transcription factor 4; PXRD, powder X-ray diffraction; Rac1, Ras-related C3 botulinum toxin substrate 1; ROS, reactive oxygen species; SEM, scanning electron microscope, microscopy; TEM, transmission electron microscope, microscopy.

Studies have related the process of epithelial-to-mesenchymal transition to CSC phenotypes. They have proven that induction of EMT in cancer could allow several stem cell-like features to concur, including self-renewal and other phenotypes of both normal and cancer stem cells (Abell and Johnson, 2014). This observation suggests that the EMT process may not only provide cancer cells with the ability to become motile and disseminate from the original site but also provide the cancer cells with the self-renewal capability that is crucial for success in clonal formation at metastatic sites (Brabletz et al., 2013; Abell and Johnson, 2014).

Several approaches have been investigated with regard to possible ways to improve cancer therapy. In the last decade, the most important archetype improvement in drug carriage was heralded by the use of nanomaterials (De Jong and Borm, 2008; Lee et al., 2017). Nanotechnology offers a variety of possibilities, including enhancement of drug delivery, facilitation of diagnostics, bioimaging, active implants, and direct therapeutic effects (Nune et al., 2009; Tomisa et al., 2011; Kadam et al., 2012; Laroui et al., 2013; Gmeiner and Ghosh, 2015). Nanosheets are an emerging class of nanomaterial with two-dimensionality (2D) and interesting properties complementing their 1D or 0D analogs (Wang and Sasaki, 2014). The sheets are flexible and highly anisotropic, and molecularly thin but microscale wide. The 2D nature could potentially lead to the effective use of surface atoms otherwise inaccessible to external stimuli. For example, $\text{Ti}_{0.8}\text{O}_2$ nanosheets derived from lepidocrocite titanate microcrystals $\text{A}_x\text{Ti}_{2-y}\text{M}_y\text{O}_4$ (Maluangnont et al., 2013) are the 2D analog of TiO_2 , possessing semiconducting, photoactive, and dielectric properties, etc. The chemical exfoliation (i.e., soft chemistry) of the microcrystals can be performed easily on a large scale at room temperature, providing a stable aqueous colloid of negatively-charged nanosheets. Their chemical compositions are derived from the microcrystals, while their lateral sizes can be controlled through exfoliating conditions (Maluangnont et al., 2013). Although nanoparticles and nanotubes of TiO_2 have been extensively studied with regard to biomedical applications, (Yin et al., 2013; Kulkarni et al., 2015) studies of $\text{Ti}_{0.8}\text{O}_2$ nanosheets are limited. For example, Song et al. (2014) recently reported *in vivo* toxicity of $\text{Ti}_{0.8}\text{O}_2$ nanosheets; a slight abnormality of the liver with increasing exposure time was observed. Here, we have performed pioneering experiments to show the selectivity of $\text{Ti}_{0.8}\text{O}_2$ nanosheets (prepared from the potassium zinc titanate precursor $\text{K}_{0.8}\text{Zn}_{0.4}\text{Ti}_{1.6}\text{O}_4$) in suppressing CSC but not normal-tissue stem cells, which could be beneficial in the development of nanomaterials for anticancer approaches.

Materials and Methods

$\text{Ti}_{0.8}\text{O}_2$ Nanosheets Synthesis. The $\text{Ti}_{0.8}\text{O}_2$ nanosheets were synthesized through a series of reactions (Maluangnont et al., 2013, 2016) consisting of solid state synthesis, proton exchange, and exfoliation as shown in Fig. 1A. The potassium zinc titanate precursor $\text{K}_{0.8}\text{Zn}_{0.4}\text{Ti}_{1.6}\text{O}_4$ was prepared by calcining the stoichiometric mixture of K_2CO_3 , ZnO and TiO_2 at 800°C for an hour, followed by grinding and another reheating at 900°C for 20 hours. The resulting white powder was subject to a repeated proton exchange (three times, overnight each; spent acid was replaced by fresh acid) with 1 M HCl at the solid-to-solution ratio of 1 g to 100 ml. The product was washed with deionized water until it was free from excess acid and was dried at room temperature overnight, giving the proton form $\text{H}_{1.6}\text{Ti}_{1.6}\text{O}_4 \cdot 0.8\text{H}_2\text{O}$. Finally, the exfoliation was accomplished by mechanically shaking the

mixture of $\text{H}_{1.6}\text{Ti}_{1.6}\text{O}_4 \cdot 0.8\text{H}_2\text{O}$ (0.4 g) and diluted tetrabutylammonium hydroxide [$(\text{C}_4\text{H}_9)_4\text{NOH}$ or TBAOH, 1 M; Sigma-Aldrich] (100 ml) at 180 rpm for 14 days, fixing the mole ratio of TBA^+ (in the solution) to H^+ (in the solid) to 1.

$\text{Ti}_{0.8}\text{O}_2$ Nanosheets Characterization. Powder X-ray diffraction (PXRD) measurements were conducted on a Rigaku DMAX 2200/Ultima+ diffractometer (Cu $\text{K}\alpha$, 40 kV, 30 mA). The mass-loss curve of the proton lepidocrocite titanate was performed using a Perkin-Elmer thermogravimetric analyzer (Pyris 1) ($\text{RT}-900^\circ\text{C}$, N_2 gas flowing at 20 ml/min). For the UV-vis measurement, the spectrum at the wavelength $\lambda = 200\text{--}600\text{ nm}$ was recorded using a T90+ UV/VIS spectrometer (PG Instruments) from a diluted colloidal suspension (0.2 ml of the original suspension, diluted to 100 ml with deionized water). The zeta potential of the nanosheets was measured by a Beckman Coulter Delsa Nano C. Microscopic images of the nanosheets were obtained from a JEOL JEM 2010 transmission electron microscope. Atomic force microscopic (AFM) images of deposited $\text{Ti}_{0.8}\text{O}_2$ nanosheets were taken with an SPA-400 system (SPA400; Seiko Instruments Inc.) in noncontact mode using a Silicon probe following the reported (Maluangnont et al., 2013) procedure.

Cell Culture and Reagents. Human non-small cell lung cancer cell lines, A549, H460, H292, and H23 cells were obtained from the American Type Culture Collection (Manassas, VA). The human keratinocyte cell line (HaCaT) was purchased from Cell Lines Service (Heidelberg, Germany). Human dermal papilla primary cell culture (primary DP1) was purchased from Celprogen (Benelux, Netherlands). Immortalized dermal papilla cells (DP) and human primary hair follicle dermal papilla cells (primary DP2) were purchased from Applied Biologic Materials Inc. (Richmond, BC). H460, H292, and H23 cells were cultivated in Roswell Park Memorial Institute (RPMI) 1640 medium (Gibco, Grand Island, NY), whereas A549, HaCaT, DP, primary DP1, and primary DP2 cells were cultivated in Dulbecco's modified Eagle's medium (Gibco). The medium was supplemented with 10% fetal bovine serum (FBS), 2 mM L-glutamine and 100 units/ml penicillin and streptomycin (Gibco, MD). Cells cultures were maintained in a 37°C humidified incubator with 5% CO_2 . Cells were routinely passaged at preconfluent density using 0.25% trypsin solution with 0.53 mM EDTA. RPMI 1640 medium, FBS, L-glutamine, penicillin/streptomycin, phosphate-buffered saline (PBS), trypsin, and EDTA were purchased from Gibco. 3-(4,5-Dimethylthiazol-2-yl)-2,5-diphenyltetrazoliumbromide (MTT), dimethyl sulfoxide, Hoechst33342, propidium iodide (PI), and bovine serum albumin, dihydroethidium (DHE), doxorubicin, and cisplatin were purchased from Sigma Chemical, Inc. (St. Louis, MO). Apoptosis Kit (FITC) was purchased from ImmunoTools (Germany). 2',7'-Dichlorofluorescein (DCF) and 3'-p-(hydroxyphenyl) fluorescein (HPF) were purchased from Invitrogen. Mn(III) tetrakis (4-benzoic acid) porphyrin (MnTBAP) was purchased from Merck (Germany). Antibodies directed against Vimentin, Snail, Slug, protein kinase B (Akt), phosphorylated protein kinase B on Ser473 [p-Akt (Ser473)], glycogen synthase kinase 3 beta (GSK3 β), phosphorylated glycogen synthase kinase 3 beta on Ser9 (p-GSK3 β (Ser 9)), Nanog, phosphorylated octamer-binding transcription factor 4 (p-Oct-4), β -catenin, Notch-1, aldehyde dehydrogenase 1 family, member A1 (ALDH1A1), Ras-related C3 botulinum toxin substrate 1 (Rac1), integrins αv , $\alpha 5$, $\beta 1$, and $\beta 3$, β -actin, and its respective secondary antibodies were purchased from Cell Signaling (Danvers, MA). Antibodies directed against prominin-1 (CD133) were purchased from Cell Applications Inc. (San Diego, CA). Antibodies directed against N-cadherin and E-cadherin were purchased from Santa Cruz Biotechnology Inc. (Dallas, TX).

Cytotoxicity Assay. For cytotoxicity assay, human lung cancer A549, H460, H292, and H23 cells, and normal cells HaCaT, DP, primary DP1, and primary DP2 cells were seeded onto 96-well plates at the density of 1×10^4 cells/well and were allowed to incubate overnight. Cells were then treated with various concentrations of $\text{Ti}_{0.8}\text{O}_2$ nanosheets for 24 hours at 37°C and analyzed for cell viability using MTT assay according to the manufacturer's protocol (Sigma Chemical). Cell viability was calculated by dividing the absorbance of

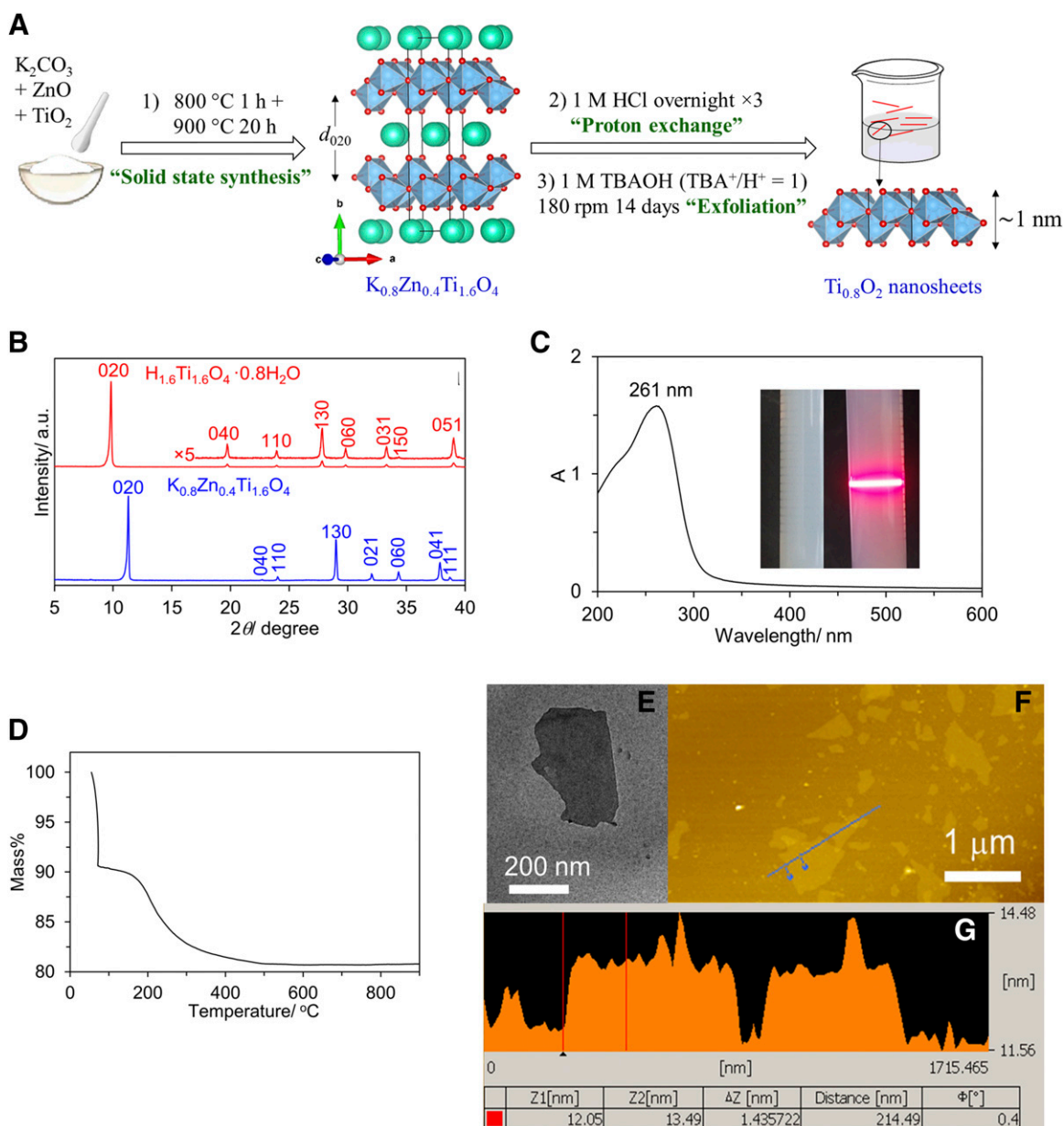


Fig. 1. The preparation of $\text{Ti}_{0.8}\text{O}_2$ nanosheets via solid state synthesis, proton exchange, and exfoliation. The crystal structure of $\text{K}_{0.8}\text{Zn}_{0.4}\text{Ti}_{1.6}\text{O}_4$ is shown as it is viewed along the *c*-direction, where K^+ ions (green) are sandwiched between the double edge-shared TiO_6 sheets (O atoms in red; Ti atoms at the center of the polyhedra) (A). The PXRD patterns of $\text{K}_{0.8}\text{Zn}_{0.4}\text{Ti}_{1.6}\text{O}_4$ and $\text{H}_{1.6}\text{Ti}_{1.6}\text{O}_4 \cdot 0.8\text{H}_2\text{O}$, with corresponding hkl indexes shown atop the peaks (B). The absorption spectrum of the $\text{Ti}_{0.8}\text{O}_2$ nanosheets, with insets showing the Tyndall effect when the laser light was shined through the colloid (C). The mass-loss curve of $\text{H}_{1.6}\text{Ti}_{1.6}\text{O}_4 \cdot 0.8\text{H}_2\text{O}$ (D) and the representative TEM image (E) and AFM image (F) with the corresponding height analysis along the line in (G).

the treated cells by that of the control cells and represented in percentage.

Nuclear Staining Assay. Nuclear costaining with Hoechst 33342 (Sigma Chemical) and propidium iodide (Sigma Chemical) was used to determine apoptotic and necrotic cell death. The human lung cancer A549 and H460, and primary DP1 cells were seeded onto 96-well plates at a density 1×10^4 cells/well, incubated overnight, and treated with $\text{Ti}_{0.8}\text{O}_2$ nanosheets at various concentration (0–10 $\mu\text{g}/\text{ml}$) for 24 hours at 37°C . Next, cells were incubated with 10 $\mu\text{g}/\text{ml}$ of Hoechst 33342 and 5 $\mu\text{g}/\text{ml}$ of PI for 30 minutes at 37°C . They were visualized and imaged under a fluorescence microscope (ECLIPSE Ts2; Nikon).

Cell Apoptosis Analysis. Apoptosis was determined with Annexin V-FITC Apoptosis Kit (ImmunoTools). The human lung cancer A549 and

H460, and primary DP1 cells were seeded in 24-well plates at a density of 1×10^5 cells/ml, incubated overnight, and treated with $\text{Ti}_{0.8}\text{O}_2$ nanosheets at various concentration (0–10 $\mu\text{g}/\text{ml}$) for 24 hours at 37°C . Cells were detached with trypsin-EDTA (0.25%), washed in PBS, and centrifuged at 1300 rpm for 5 minutes. Cells were suspended in 100 μl of $1\times$ binding buffer and incubated in 5 μl of annexin V-FITC and 1 μl of PI for 15 minutes at room temperature in the dark. Five hundred microliters of incubation buffer were added, and cells were analyzed by guava easyCyte flow cytometry systems.

Scanning Electron Microscopy Morphologic Analysis. H460-treated cells were fixed in 2.5% glutaraldehyde in 0.1 M phosphate buffer pH 7.2 for 1–2 hours. Cells were rinsed twice with phosphate buffer and once with distilled water for 5 minutes each. Cells were dehydrated with a graded series of ethanol (30%, 50%, 70%,

and 95% for 5 minutes each and 100% three times, 5 minutes/time), dried, mounted, and coated with gold (sputter coater, Balzers model SCD 040, Germany). After that, Cells were observed under a scanning electron microscope (SEM; model JSM6400; JEOL, Tokyo, Japan).

Cellular Uptake Analysis. H460 and primary DP1 cells (1×10^6 cells/ml) were seeded in 10-cm dishes and treated with TiO_2S_2 nanosheets at $1 \mu\text{g/ml}$ for 24 hours. The treated cells were collected, washed with PBS, and then fixed in 2% glutaraldehyde, post-fixed in 1% osmium tetroxide, dehydrated in alcohol, and embedded. Thin sections of resin-embedded H460 and primary DP1 cells were cut, and cellular uptake was observed with a transmission electron microscope (TEM) JEM-1400 (Jeol Ltd.).

Migration Assay. Human NSCLC-derived cells (H460 and A549) and primary DP1 cells were pretreated with TiO_2S_2 nanosheets at nontoxic concentrations (0 to $1 \mu\text{g/ml}$) for 48 hours at 37°C . The treated cells were then seeded onto 96-well plates at a density of 3×10^4 cells/well. Monolayer cells were next allowed to migrate after the attached cells were scratched with a P200 micropipette tip to generate a wound space. Four random fields of the wound space were examined and imaged under a phase-contrast microscope (ECLIPSE Ts2; Nikon) at various time points (0, 24, and 48 hours). Relative cell migration was quantified by dividing the percentage change of the wound space in treated cells to that of the control cells. For the Transwell assay, the treated cells (A549, H460, and primary DP1 cells) were seed at a density of 3×10^4 cells/well in the upper chamber supplemented with serum-free medium (8- μm pore size) in a 24-well plate. The lower chamber was filled with complete medium containing 10% FBS as a chemoattractant. After 24 hours, the nonmigrated cells in upper chamber were removed by cotton-swab, and the cells that migrated to the underside of the membrane were fixed with cold methanol for 10 minutes and stained with $10 \mu\text{g/ml}$ of Hoechst 33342 for 10 minutes. The stained cells were visualized and scored under a fluorescence microscope (ECLIPSE Ts2).

Invasion Assay. This assay was performed using chambers with 8- μm pore filter inserts in 24-well plates (Corning Life Sciences). The upper chamber of the inserts was coated with $50 \mu\text{l}$ of 0.5% Matrigel from BD Biosciences (San Jose, CA). Human NSCLC-derived cells (H460 and A549) and primary DP1 cells were pretreated with TiO_2S_2 nanosheets at nontoxic concentrations (0 to $1 \mu\text{g/ml}$) for 48 hours at 37°C . The treated cells were seeded at a density of 3×10^4 cells/well in the upper chamber supplemented with serum free medium. The lower chamber was filled with complete medium containing 10% FBS as a chemoattractant. After 24 hours, the noninvading cells in the upper chamber were removed with a cotton swab and the invading cells in the lower chamber were fixed with cold methanol for 10 minutes and stained with $10 \mu\text{g/ml}$ of Hoechst 33342 for 10 minutes. The stained cells were then visualized and scored under a fluorescence microscope (ECLIPSE Ts2; Nikon).

Anchorage-Independent Growth Assay. Anchorage-independent cell growth was determined by soft agar colony formation assay. Human NSCLC-derived cells (H460 and A549) and primary DP1 cells were pretreated with TiO_2S_2 nanosheets at nontoxic concentrations (0 to $1 \mu\text{g/ml}$) for 48 hours at 37°C . Soft agar was prepared by using a 1:1 mixture of cultured medium containing 10% FBS and 1% agarose. The mixture was allowed to solidify in a 24-well plate to form a bottom layer, after which an upper cellular layer consisting of 3×10^3 cells/ml in the agarose gel with 10% FBS and 0.33% agarose was added. After the upper layer was solidified, the system was added with cultured medium containing 10% FBS and incubated at 37°C . Colony formation was determined after 2 and 3 weeks using a phase-contrast microscope (ECLIPSE Ts2; Nikon). Relative colony number and diameter were determined the values of the treated cells dividing by control cells.

Spheroids Formation Assay. Spheroids were grown using the adjusted method from Chanvorachote and Luanpitpong (2016), Phiboonchaiyanan et al. (2016), and Powan et al. (2017). Human NSCLC-derived cells (H460 and A549) and primary DP1 cells were pretreated with TiO_2S_2 nanosheets at nontoxic concentrations (0– $1 \mu\text{g/ml}$) for 48 hours at 37°C . The treated cells at a density

of 2.5×10^3 cells/well were seeded onto an ultralow-attachment plate in 0.8% methylcellulose-based serum-free medium supplemented with 20 ng/ml epidermal growth factor, 4 mg/ml insulin, and basic fibroblast growth factor for 7 days to form primary spheroids. Then the primary spheroids were detached using 1 mM EDTA and suspended into single cells. These cells were grown in a 24-well ultralow-attachment plate at a density of 2.5×10^3 cells/well in 0.8% methylcellulose-based serum-free medium supplemented with 20 ng/ml epidermal growth factor, 4 mg/ml insulin, and basic fibroblast growth factor for 21 days to form secondary spheroids. At days 14 and 21, the numbers and sizes of secondary spheroids were determined and imaged using a phase-contrast microscopy (ECLIPSE Ts2; Nikon).

For CSC-rich population formation, the method was slightly modified from a previously described method (Chanvorachote and Luanpitpong, 2016; Phiboonchaiyanan et al., 2016; Powan et al., 2017). Cells were seeded onto a 24-well ultralow-attachment plate, with approximately 2.5×10^3 cells/well in 0.8% methylcellulose-based serum-free medium supplemented with 20 ng/ml epidermal growth factor, basic fibroblast growth factor, and 4 mg/ml insulin. The primary spheroids were allowed to form for 7 days. At day 7 of primary spheroid culture, primary spheroids were resuspended into single cells using 1 mM EDTA, and again 2.5×10^3 cells/well were seeded onto a 24-well ultralow-attachment plate. Secondary spheroids were allowed to form for 14 days.

The single three-dimensional spheroid formation assay cells were then allowed to form primary and secondary spheroids as detailed above. After 14 days, secondary spheroids were dissociated into the same size. Each single secondary spheroid was transferred at one spheroid per well to a 24-well ultralow-attachment plate and subjected to treatment with or without TiO_2S_2 nanosheets for 7 days in 0.8% methylcellulose-based serum-free medium supplemented with 20 ng/ml epidermal growth factor, 4 mg/ml insulin, and basic fibroblast growth factor in medium. At 0, 3, 5, 7 days of treatment the secondary spheroid sizes were determined and imaged using phase-contrast microscopy (ECLIPSE Ts2; Nikon).

Enzyme-Limiting Dilution Assay. This study was slightly modified from previously described methods (Slifka and Ahmed, 1996). Cells were plated in gradually decreasing number from 100 to 1 cell/well onto a 96-well ultralow-attachment plate and cultured for 14 days, and the number of spheroid was recorded. The treated spheroids were calculated in all wells compared with the control.

Cell Aggregation Behavior Evaluation. Cells were seeded in a 24-well plate at 6×10^3 cells/well and incubated overnight for cell attachment. The cells were then treated with various concentrations of TiO_2S_2 nanosheets (0 to $1 \mu\text{g/ml}$) for 72 hours. After exposure to the treatments, aggregation behavior of cells was determined at 72 hours. Aggregation behavior of cells was photographed by a phase-contrast microscope (ECLIPSE Ts2; Nikon).

Intracellular Reactive Oxygen Species Determination. The intracellular reactive oxygen species (ROS), hydroxyl radical, and superoxide anion production were determined by flow cytometry using DCF, HPF, and DHE as fluorescent probes. In brief, cells were seeded into 24-well plates at a density of 3.0×10^4 cells per well and treated with 0.5 and $1 \mu\text{g/ml}$ of TiO_2S_2 nanosheets for 24 hours. After treatment, the cells were washed with cold PBS and then incubated with $10 \mu\text{M}$ DCF, $10 \mu\text{M}$ HPF, or $10 \mu\text{M}$ DHE for 30 minutes for the detection of intracellular ROS, hydroxyl radical, and superoxide anion, respectively. The fluorescence intensity of DCF, HPF, and DHE were detected by flow cytometric analysis.

Western Blot Analysis. After TiO_2S_2 nanosheets treatment, human NSCLC-derived cells (H460 and A549) and primary DP1 cells were incubated with lysis buffer containing 20 mM TrisHCl (pH 7.5), 1% Triton X-100, 150 mM sodium chloride, 10% glycerol, 1 mM sodium orthovanadate, 50 mM sodium fluoride, 100 mM phenylmethylsulfonyl fluoride, and protease inhibitor cocktail (Roche Molecular Biochemical) for 30 minutes on ice. The cellular lysates were collected and their protein content was determined using a BCA protein assay kit (Pierce Biotechnology, Rockford, IL). Equal amounts of protein from each

sample were separated by SDS-PAGE and transferred to 0.45- μm nitrocellulose membranes (Bio-Rad). The resulting blots were blocked for 1 hour with 5% nonfat dry milk in TBST (Tris-buffer saline with 0.1% Tween containing 25 mM Tris-HCl, pH 7.5, 125 mM NaCl, and 0.1% Tween 20) and incubated with specific primary antibodies against Vimentin, Snail, Slug, Akt, p-Akt (Ser473), GSK3 β , p-GSK3 β (Ser 9), Nanog, p-Oct-4, β -catenin, Notch-1, ALDH1A1, Rac1, Integrin αv , α5 , β1 and β3 , and β -actin at 4°C overnight. After three washes in TBST, the blots were incubated with horseradish peroxidase-conjugated secondary antibodies for 2 hours at room temperature. Finally, protein bands were detected using an enhanced chemiluminescence substrate (Supersignal West Pico; Pierce) and exposed to film.

Flow Cytometry Analysis. Cells were harvested by centrifugation after which the resuspend cells were incubated on ice with a rabbit anti-CD133 antibody or an anti-ALDH1A1 antibody for 1 hour. Next, the primary antibodies were removed and the cells were washed and incubated for 30 minutes with Alexa Flour 488 (Invitrogen)-conjugated goat anti-rabbit IgG (H+L) secondary antibody. After a washing, the fluorescence intensity was determined by flow cytometry using a 488 nm excitation and a 519-nm band-pass filter. The mean fluorescence intensity was quantified using guava easyCyte flow cytometry systems.

Immunofluorescence. Cells were seeded onto 96-well plates at the density of 1×10^5 cells/well. After treatment for 48 hours, the cells were fixed with 4% (w/v) paraformaldehyde for 30 minutes and permeabilized with 0.1% (v/v) Triton-X for 20 minutes. The cells were next incubated with 3% (w/v) bovine serum albumin for 30 minutes, washed, and incubated with an anti-N-cadherin or anti-E-cadherin antibody overnight at 4°C, washed, and incubated with Alexa Flour 488 (Invitrogen)-conjugated goat anti-rabbit IgG (H+L) secondary antibody for 1 hour at room temperature in the dark. Thereafter, the cells were washed with PBS, costained with 10 $\mu\text{g/ml}$ Hoechst 33342, and visualized and imaged using fluorescence microscopy (ECLIPSE Ts2; Nikon).

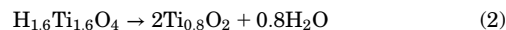
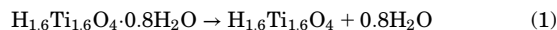
Statistical Analysis. Data from three or more independent experiments are presented as mean \pm S.D. Multiple comparisons for statistically significant differences between multiple groups were performed using analysis of variance, followed by individual comparisons with Scheffe's post-hoc test. Statistical significance was considered at $P < 0.05$.

Results

Characterization of $\text{K}_{0.8}\text{Zn}_{0.4}\text{Ti}_{1.6}\text{O}_4$ and $\text{H}_{1.6}\text{Ti}_{1.6}\text{O}_4 \cdot 0.8\text{H}_2\text{O}$ Nanosheet. The PXRD patterns of $\text{K}_{0.8}\text{Zn}_{0.4}\text{Ti}_{1.6}\text{O}_4$ and $\text{H}_{1.6}\text{Ti}_{1.6}\text{O}_4 \cdot 0.8\text{H}_2\text{O}$ in Fig. 1B are characteristic of compounds with a lepidocrocite structure, (Sasaki and Watanabe, 1998; Maluangnont et al., 2016, 2017), thereby confirming a successful synthesis. As shown in Fig. 1A, $\text{K}_{0.8}\text{Zn}_{0.4}\text{Ti}_{1.6}\text{O}_4$ is built from the sheets of double edge-shared $(\text{Ti/Zn})\text{O}_6$ octahedra interleaved by K^+ ions. The distance d_{020} is the intersheet separation. The shift of the d_{020} from $d = 0.78$ nm ($2\theta \sim 11.3^\circ$) to $d = 0.90$ nm ($2\theta \sim 9.8^\circ$) as a result of proton exchange indicates (Sasaki and Watanabe, 1998) the notable interlayer expansion resulting from the incorporation of a water molecule between the sheets.

Since the dissolution of zinc by acid is well known, the proton exchange of $\text{K}_{0.8}\text{Zn}_{0.4}\text{Ti}_{1.6}\text{O}_4$ to $\text{H}_{1.6}\text{Ti}_{1.6}\text{O}_4 \cdot n\text{H}_2\text{O}$ was first assumed. Here, a 1:1 exchange of protons for K^+ ions, and a 2:1 exchange for Zn^{2+} ions can be expected. The number of water molecules (n) can be calculated from the mass-loss curve (Fig. 1D) assuming the thermal transformations below. By employing formula weights of 156.592 g/mol for $\text{H}_{1.6}\text{Ti}_{1.6}\text{O}_4 \cdot 0.8\text{H}_2\text{O}$ and 18 for water, the mass loss in both eqs. (1) and (2) equals $(0.8 \times 18/156.592) \times 100\% = 9.20\%$, which is

in reasonable agreement with the observed mass losses in the first (9.5%) and second (9.0%) steps.



The $\text{H}_{1.6}\text{Ti}_{1.6}\text{O}_4 \cdot 0.8\text{H}_2\text{O}$ powder was next exfoliated with TBAOH. The mixture, which initially containing the suspended powder and a clear liquid, gradually transformed into a white translucent colloid, as shown in the left inset of Fig. 1C. This colloid exhibited a Tyndall effect whereby the light was scattered throughout, as shown in the right inset. These observations suggest (Sasaki and Watanabe, 1998; Maluangnont et al., 2013) the infinite separation (i.e., exfoliation) of stacks of layers in the proton-containing lepidocrocite titanate into elementary units. The colloid absorbed light at $\lambda_{\text{max}} \sim 261$ nm (Fig. 1C), which is also in good agreement with the literature (Sasaki and Watanabe, 1998). The zeta potential of the nanosheets (-30 mV) confirmed that they are negatively charged, as one would expect considering the stoichiometry of the titanate precursor.

Figure 1E is the representative TEM image showing a flat 2D nanosheet with uniform contrast. The presence of nanosheets was further supported by the AFM image and the corresponding height analysis, shown in Fig. 1, F and G. The 2D objects with a wide distribution of lateral sizes (maximum $\sim 1 \times 1$ μm) and a height of approximately 1.4 nm can be clearly observed. Although the crystallographic thickness in the b direction (i.e., of the layer) is ~ 0.75 nm, (Sasaki and Watanabe, 1997) the reported thickness of ~ 1.4 nm is probably the result of adsorption of water molecules and/or TBA^+ on the surface.

Cytotoxicity of $\text{Ti}_{0.8}\text{O}_2$ Nanosheets on Cancerous Human Lung Cells and Normal Cells. Cells were treated with various concentrations of $\text{Ti}_{0.8}\text{O}_2$ nanosheets (0–100 $\mu\text{g/ml}$) and analyzed for cell viability. The results showed that statistically significant cytotoxic effects of $\text{Ti}_{0.8}\text{O}_2$ nanosheets could be found at the concentrations of 0.05–100 $\mu\text{g/ml}$ in H23 cells; 5–100 $\mu\text{g/ml}$ in H460, H292, and HaCaT cells; 10–100 $\mu\text{g/ml}$ in A549 and DP cells; and 50–100 $\mu\text{g/ml}$ in primary DP1 and primary DP2 cells (Fig. 2, A–H). Apoptosis assay revealed that treatment with 10 $\mu\text{g/ml}$ $\text{Ti}_{0.8}\text{O}_2$ nanosheets mediated apoptosis in lung cancer cells (Fig. 2, I, J, L, and M), whereas it had no toxic effect on primary DP1 cells (Fig. 2, K–M). Flow cytometry analysis using annexin V/PI detection as a basis also confirmed that 10- $\mu\text{g/ml}$ $\text{Ti}_{0.8}\text{O}_2$ nanosheets induced dramatic apoptosis in A549 and H460 cells but only had a minimal effect on primary DP1 cells (Fig. 2, N–P). Furthermore, SEM morphologic analysis demonstrated that 10- $\mu\text{g/ml}$ $\text{Ti}_{0.8}\text{O}_2$ nanosheets initially changed the morphology, including the formation of stress fibers (Fig. 2Q). In addition, TEM analysis showed that $\text{Ti}_{0.8}\text{O}_2$ nanosheets can sufficiently enter into the cancer and normal primary DP1 cells (Fig. 2R).

$\text{Ti}_{0.8}\text{O}_2$ Nanosheets Suppress Cancer Stem Cell-Like Phenotypes. The ability of cancer cells to form tumor spheroids and grow in an anchorage-independent condition was shown to be a hallmark of cancer stemness as well as metastatic potential (Wang et al., 2017). We further investigated the effect of $\text{Ti}_{0.8}\text{O}_2$ nanosheets on the growth of A549 and H460 cells and primary DP1 under this condition. Figure 3, A–D, demonstrates that treatment of A549 and H460 cells with nontoxic concentrations of $\text{Ti}_{0.8}\text{O}_2$ nanosheets

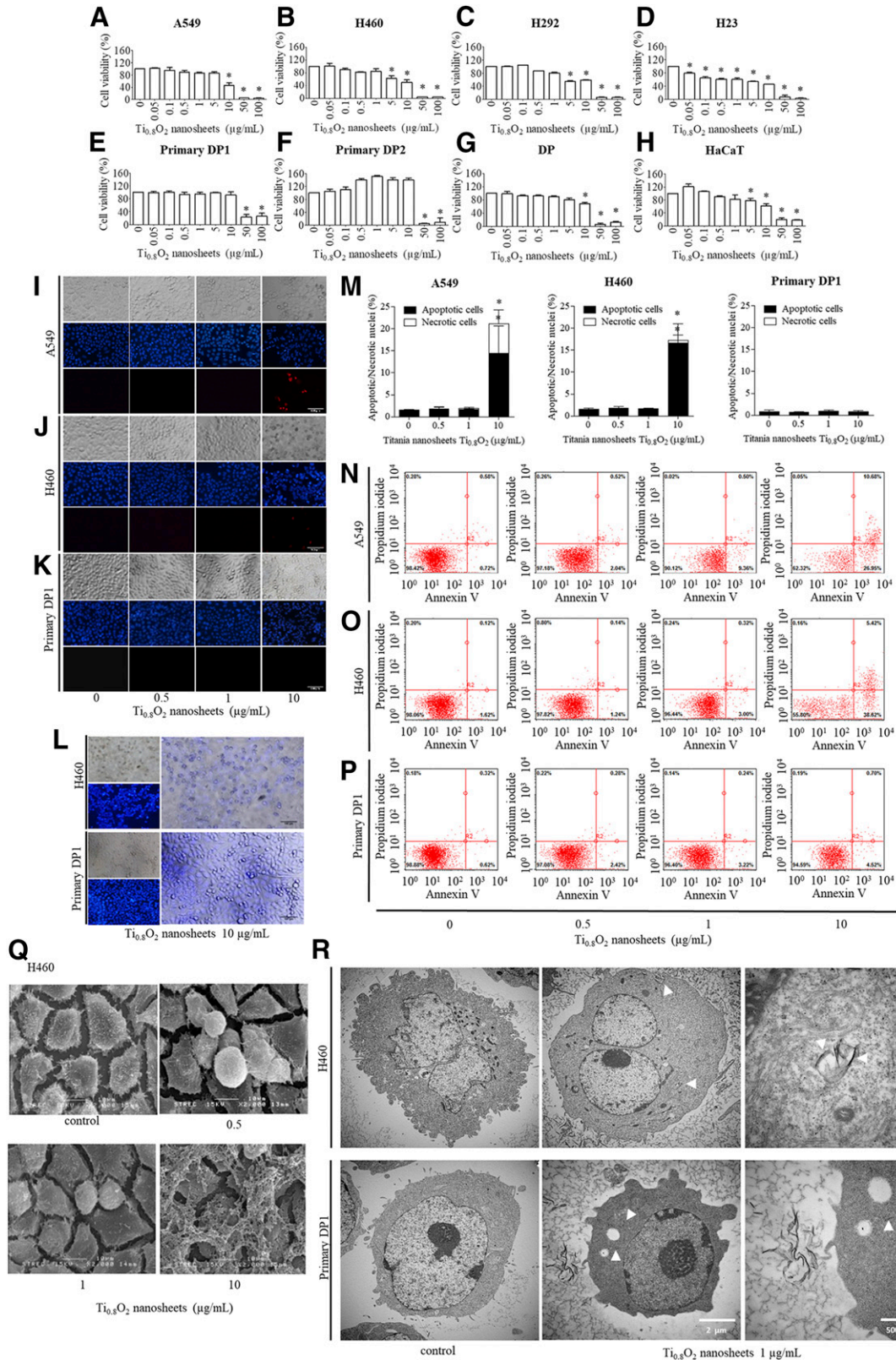


Fig. 2. The cytotoxic effect of TiO_2O_2 nanosheets on lung cancer and normal cells. Effect of TiO_2O_2 nanosheets on cell viability of lung cancer cells (A549, H460, H292, and H23) and normal cells [dermal papilla (DP) cell line, primary DP1, primary DP2, and HaCaT keratinocyte cells] for 24 hours using MTT assays (A–H). Apoptotic and necrotic nuclei in cells treated with TiO_2O_2 nanosheets, determined by Hoechst 33342/PI costaining and visualized using fluorescence microscopy (I–M). Annexin/PI costained cells were determined by flow cytometry (N–P). Morphology of H460 cells was determined using SEM (Q). TEM pictures of the cellular uptake of TiO_2O_2 nanosheets in H460 and primary DP cells at 24 hours (R). Data are shown as the mean \pm S.D. ($n = 3$). * $P < 0.05$ vs. nontreated control.

decreased the formation of cancer cell colonies in terms of number and diameter of colonies, in a dose-dependent manner, in comparison with the control. On the other hand, treatment of primary DP1 cells with nontoxic concentrations of $\text{Ti}_{0.8}\text{O}_2$ nanosheets slightly increased colony number and not altered colony size (Fig. 3, E and F).

Our finding was confirmed by a spheroid formation assay showing that the $\text{Ti}_{0.8}\text{O}_2$ nanosheet-treated cells (A549 and H460 cells) exhibited a decreased spheroid-forming ability, with a statistically significant decrease in both spheroid number and diameter in comparison with nontreated control cells (Fig. 3, G–J), but $\text{Ti}_{0.8}\text{O}_2$ nanosheets could not alter spheroid number and diameter of primary DP1 cells (Fig. 3, K and L). Extreme limiting-dilution assay also showed that the nontreated controls exhibited the ability of cells to form spheroids, whereas the nanosheet-treated cells were able to attenuate spheroid formation (Fig. 3, M and N). Further, we found that $\text{Ti}_{0.8}\text{O}_2$ nanosheets decreased the size of the spheroid in both A549 and H460 cells as early as 3 days following the treatment (Fig. 3, O–R).

Having shown that $\text{Ti}_{0.8}\text{O}_2$ nanosheets could suppress CSC-like phenotypes in lung cancer cells, we next investigated the possible mechanism by which such nanosheets could attenuate these features. First, we attempted to explain the CSC-suppressing effect of nanosheets by determining the cellular level of the well known stem cell markers CD133 and ALDH1A1, and stem cell-regulating transcription factors such as Nanog and p-Oct-4. Western blotting revealed that $\text{Ti}_{0.8}\text{O}_2$ nanosheets diminished the CD133 and ALDH1A1 in A549 and H460 (Fig. 4, A and C) cells but had only minimal affect on such proteins in DP1 cells (Fig. 4E). Results indicated that the expression levels of stem cell markers in primary DP1 cells had not altered in response to nanosheets (0.1–1 $\mu\text{g}/\text{ml}$) (Fig. 4E). Like results were observed when we detected the stem cell transcription factors. Treatment of lung cancer cells with nanosheets decreased the levels of p-Oct4 and Nanog (Fig. 4, A and C) but $\text{Ti}_{0.8}\text{O}_2$ nanosheets did not alter such proteins in DP1 cells (Fig. 4E).

Just as in normal tissue stem cells, several cell-signaling pathways have been implicated in mechanisms underlying stemness in CSCs. Protein kinase B (Akt), β -catenin, and Notch signals have been shown to be key regulatory mechanisms underlying stemness in both normal and cancerous stem cells (Hadjimichael et al., 2015; Mohammed et al., 2016; Phiboonchaiyanan et al., 2016; Koury et al., 2017). To clarify the possible effects of nanosheets on such stem cell pathways, we determined the levels of related proteins in nanosheet-treated cells. Figure 4, A and C, show that treatment with $\text{Ti}_{0.8}\text{O}_2$ nanosheets decreased the level of Notch1 in A549 and H460 cells, but it had no effect on such protein level in primary DP1 cells (Fig. 4E). CSCs also enhance and maintain their phenotypes through the Akt signaling pathway (Xia and Xu, 2015) and stabilization of CSC regulatory protein β -catenin (Ma et al., 2013). We found that treatment with $\text{Ti}_{0.8}\text{O}_2$ nanosheets decreased the active Akt (phosphorylated Akt at Ser473). Active Akt can suppress the function of GSK3 β in mediating β -catenin degradation, via phosphorylated GSK3 β at Ser9 (Fukumoto et al., 2001). In A549 and H460 cells (Fig. 4, B and D), we found that both p-Akt and p-GSK3 β (Ser9) were depleted in response to the treatment, whereas the levels of p-Akt and p-GSK3 β (Ser9) in primary DP1 cells were not altered (Fig. 4F). Consequently, the level of β -catenin, a

mediator for self-renewal and tumorigenic properties, (Jiang et al., 2016) was downregulated in the nanosheet-treated cells (Fig. 4, B and D). To confirm, the CD133 and ALDH1A1-positive cells were evaluated by flow cytometry in A549 and H460 lung cancer cells and in primary DP cells. Although the number of CD133 and ALDH1A1-positive cells was reduced in both types of lung cancer cell by nanosheet treatment (Fig. 4, G and H), the population of those CD133- and ALDH1A1-stained cells was not altered in primary DP1 cells (Fig. 4I). Taken together, these results enabled us to unravel the pivotal data indicating that $\text{Ti}_{0.8}\text{O}_2$ nanosheets attenuate stem-cell properties and signaling in lung cancer cells, but not in normal primary DP cells, via Akt/ β -catenin and Notch1 suppression. Moreover, the A549 cells were treated with cisplatin and doxorubicin, standard chemotherapeutic drugs for lung cancer. For comparison, the cytotoxicity of nanosheet, cisplatin, and doxorubicin was determined (Fig. 4J). The result showed that both cisplatin and doxorubicin enriched CSC, as indicated by the increase of CSC markers such as ALDH1A1, Notch1, β -catenin, and p-Akt (Fig. 4K).

$\text{Ti}_{0.8}\text{O}_2$ Nanosheets Weaken EMT and Reduce Metastasis-Related Integrins. EMT, or transition of an epithelial phenotype to a more mesenchymal phenotype of cancer cell, is another exploitable pathway of augmentation-aggressive activity of cancer. EMT involves the alteration of proteins, including the E-cadherin to N-cadherin switch (Gravdal et al., 2007) and increase of vimentin, Snail, and Slug (Medici et al., 2008; Liu et al., 2015). We next explored whether $\text{Ti}_{0.8}\text{O}_2$ nanosheets could suppress EMT in lung cancer cells. Treatment of the cells (A549 and H460) with $\text{Ti}_{0.8}\text{O}_2$ nanosheets caused a decrease in the level of N-cadherin and an increase in the level of E-cadherin, in a dose-dependent manner (Fig. 5, A and C). Immunofluorescence staining supports our finding that $\text{Ti}_{0.8}\text{O}_2$ nanosheets caused a decrease in the level of N-cadherin and an increase in the level of E-cadherin (Fig. 5, G and H). $\text{Ti}_{0.8}\text{O}_2$ nanosheet caused similar effects on the levels of N-cadherin and E-cadherin in primary DP1 cells (Fig. 5E). In addition, $\text{Ti}_{0.8}\text{O}_2$ nanosheets dramatically reduced the EMT-related proteins of Vimentin, Slug, Snail, and Rac1 in a dose-dependent manner in A549 and H460 cells (Fig. 5, A and C). However, only Snail was found to decrease in primary DP1 cells (Fig. 5E).

It is worth noting that several reports have pointed out the critical role of certain integrins (including αv , $\alpha 5$, $\beta 1$ and $\beta 3$) that enhance the metastasis potential of cancer cells (Canel et al., 2013). The levels of the αv , $\alpha 5$, $\beta 1$, and $\beta 3$ integrins were therefore evaluated by Western blot analysis. We found that treatment with $\text{Ti}_{0.8}\text{O}_2$ nanosheets decreased the expression of integrins αv and $\beta 1$ in A549 and H460 cells and primary DP1 cells, whereas the expression of integrins $\alpha 5$ and $\beta 3$ was not changed (Fig. 5, D and F). Here, we have shown the additional benefits of using $\text{Ti}_{0.8}\text{O}_2$ nanosheets for inhibition of metastasis by suppressing EMT and decreasing the αv and $\beta 1$ integrins. In addition, the Akt/GSK3 β signaling pathway is not only implicated in mechanisms underlying stemness in CSCs but also in regulating the stability and transcription activity of Snail/Slug, repressing E-cadherin, and inducing EMT.

$\text{Ti}_{0.8}\text{O}_2$ Nanosheets Decrease Cell Migration and Invasion. The ability of cancer cells to migrate and invade has been observed in the characterizations of CSCs, EMT, and

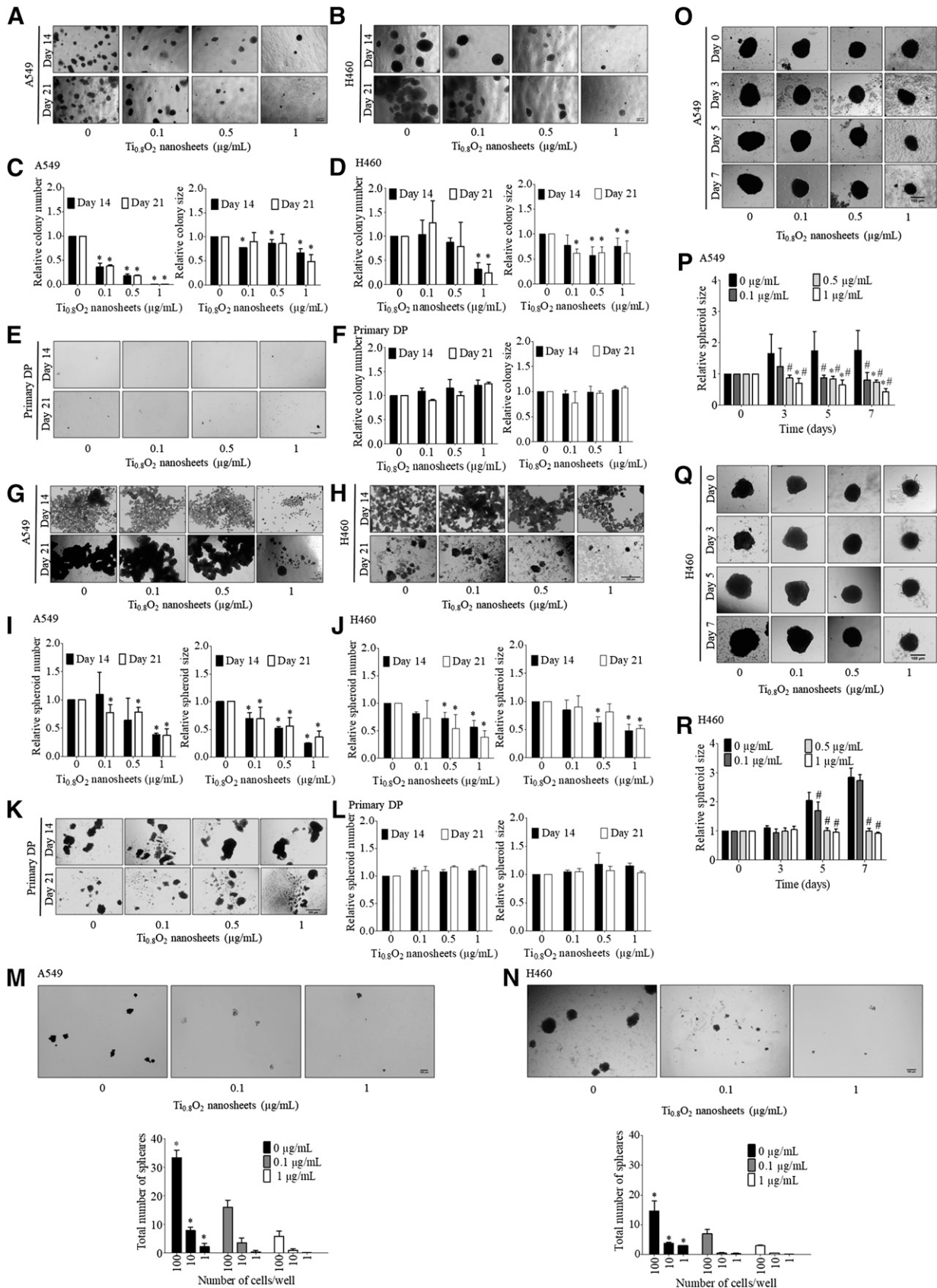


Fig. 3. TiO_2O_2 nanosheets decrease anchorage-independent growth and suppress CSC-like phenotypes and CSC growth in CSC-rich populations in lung cancer cells. A549, H460, and primary DP1 cells were treated with TiO_2O_2 nanosheets (0–1 $\mu\text{g}/\text{mL}$) for 48 hours. The treated cells were subjected to anchorage-independent growth assays for 2 and 3 weeks (A, B, and E), and assessed by microscopy ($4\times$). The colony number as a percentage and the size of the treated cell were analyzed and compared with the control (C, D, and F). TiO_2O_2 nanosheets decreased spheroid formation of A549, H460, and primary

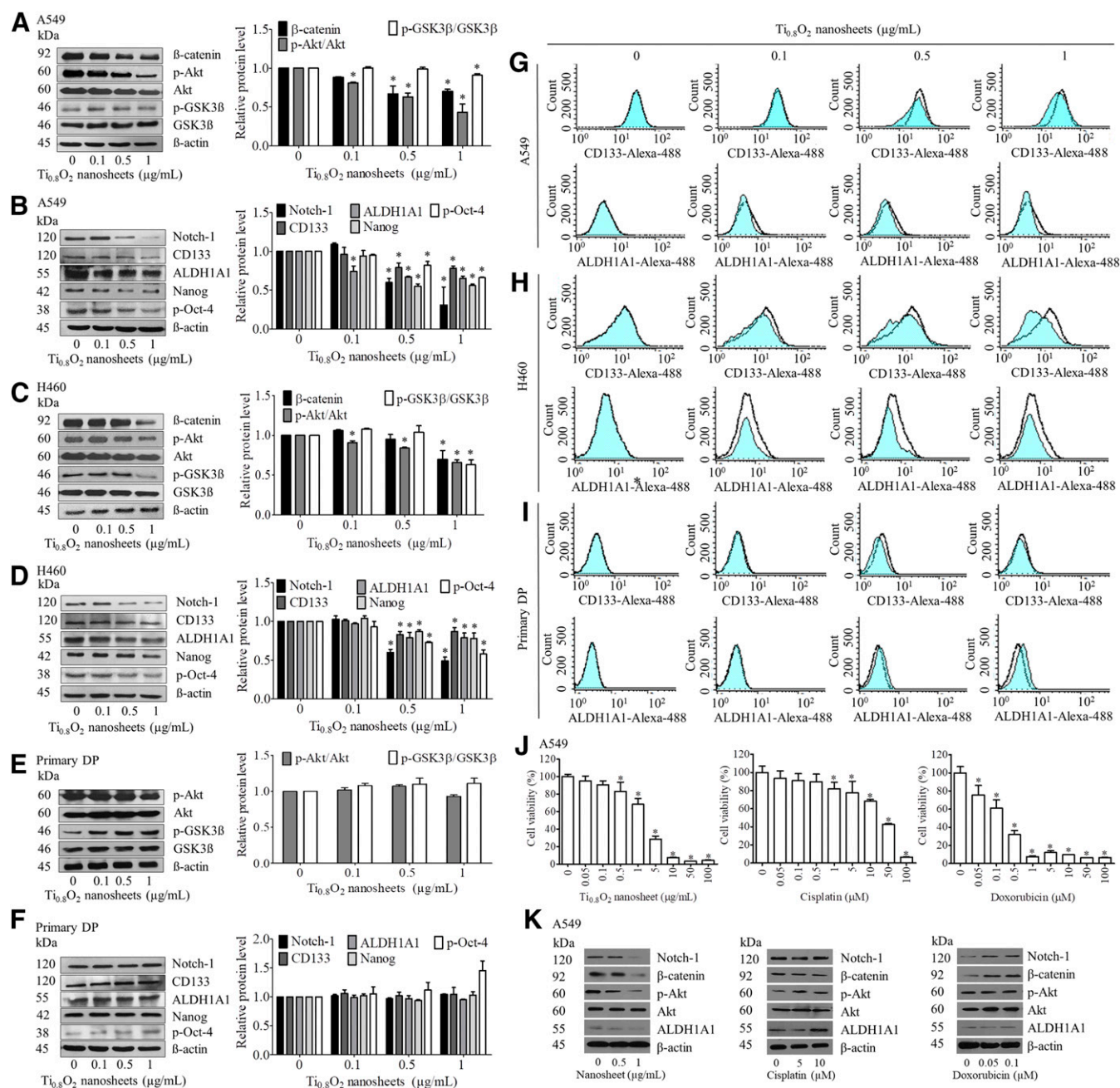


Fig. 4. TiO₂O₂ nanosheets inhibit the expression of CSC markers and self-renewal transcription-factor proteins. A549, H460, and primary DP1 cells were treated with TiO₂O₂ nanosheets (0–1 μg/ml) for 48 hours. The expression levels of CSC protein markers in A549, H460 (A–D), and primary DP1 (E and F) were determined by Western blotting. CD133 and ALDH1A1 expression levels were measured by flow cytometry (G–I). Effect of TiO₂O₂ nanosheets, cisplatin, and doxorubicin on cell viability of A549 cells for 24 hours using MTT assays (J) and their effects on protein expression levels of CSC protein markers in A549 cells (K).

metastatic cancer cells (Abell and Johnson, 2014). We further evaluated whether TiO₂O₂ nanosheets could attenuate such aggressive behaviors of cancer cells. Figure 6, A and B, show that TiO₂O₂ nanosheets inhibited cell migration of A549 and H460 cells. Analysis of cell migration and

invasion, carried out with Boyden chambers, consistently demonstrated that TiO₂O₂ nanosheets were able to decrease the number of A549 and H460 cells migrating and invading across the Transwell filter within 24 hours in a dose-dependent manner, in comparison with the control,

DP1 cells after 2 and 3 weeks (G, H, and K), according to microscopy assessment (4×). The relative spheroid number and size, compared with those of the untreated controls (I, J, and L). The CSC-rich cells of A549 and H460 cells were treated with TiO₂O₂ nanosheets and plated in decreasing numbers from 100 cells/well to 1 cell/well for 14 days (M and N). The single CSC-rich spheroids were treated with TiO₂O₂ nanosheets for 3, 5, and 7 days (O and Q), and the relative spheroid sizes compared with those of untreated controls were monitored (P and R). Data are shown as the mean ± S.D. (n = 3). *P < 0.05 vs. nontreated control. The relative spheroid sizes were investigated by comparing with nontreated control in each time. #P < 0.05 vs nontreated control in each time.

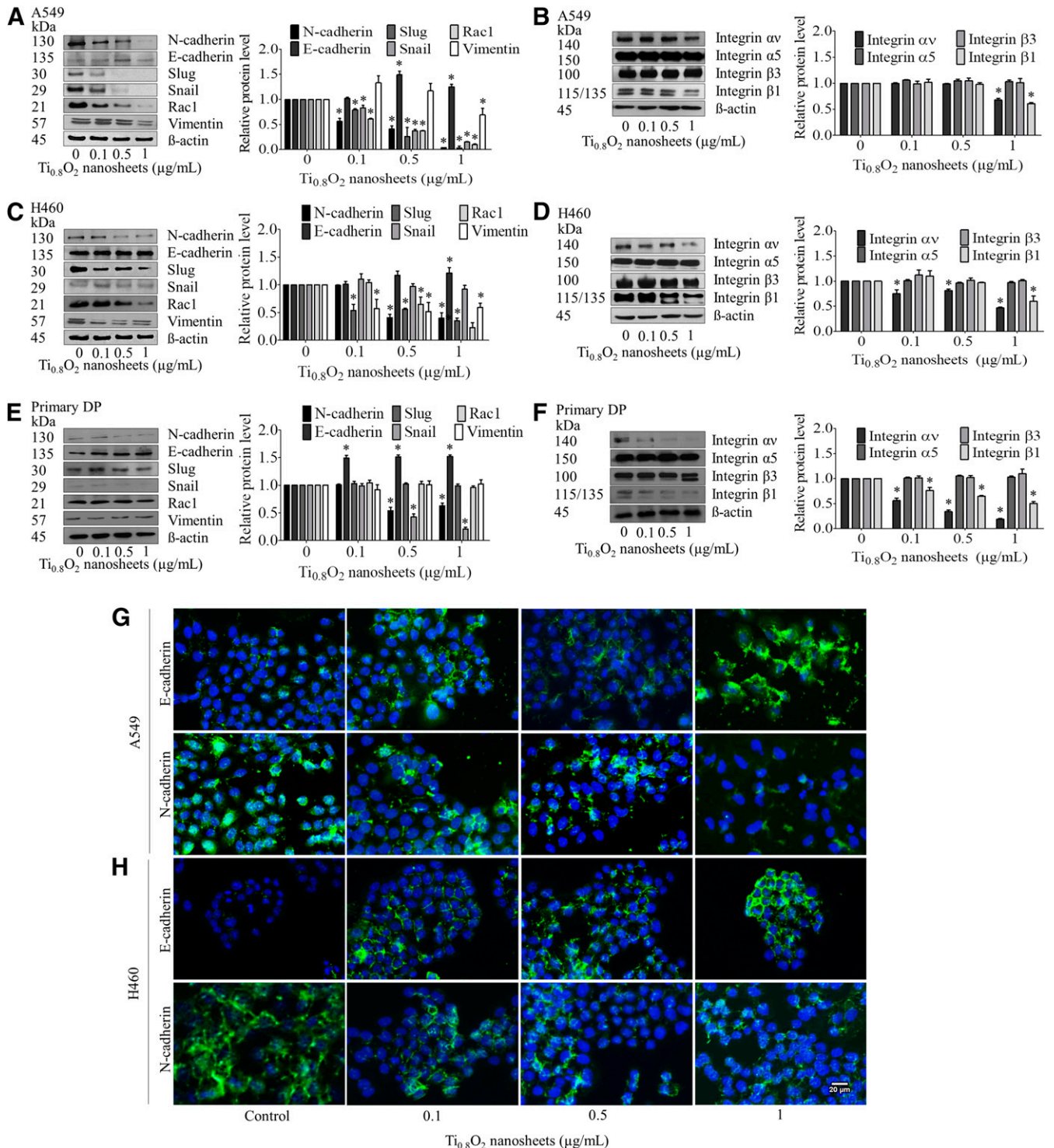


Fig. 5. Effect of $\text{Ti}_{0.8}\text{O}_2$ nanosheets on EMT. A549, H460, and primary DP1 cells were treated with $\text{Ti}_{0.8}\text{O}_2$ nanosheets (0–1 $\mu\text{g/mL}$) for 48 hours. The expression levels of EMT protein markers and integrins were investigated by Western blotting (A–F). Blots were reprobed with β -actin to confirm equal loading of samples. The immunoblot signals were quantified by densitometry, and the mean data from independent experiments were normalized to the results. Data are shown as the mean \pm S.D. ($n = 3$). * $P < 0.05$ vs. nontreated control. Expression of E-cadherin and N-cadherin was analyzed by immunofluorescence staining (G and H).

but $\text{Ti}_{0.8}\text{O}_2$ nanosheets had no effect on the motility of primary DP1 cells (Fig. 6, C and D).

$\text{Ti}_{0.8}\text{O}_2$ Nanosheets Have No Effect on Primary Dermal-Papilla Aggregation Properties. The data thus far has indicated that DP aggregation patterns reflect the

ability to form hair (Sari et al., 2016). Having shown the promising effect of $\text{Ti}_{0.8}\text{O}_2$ nanosheets in selective suppression of the CSC in lung cancer, we next evaluated whether treatment of normal cells with such a substance affected the viability of normal cells as well as their stem cell properties.

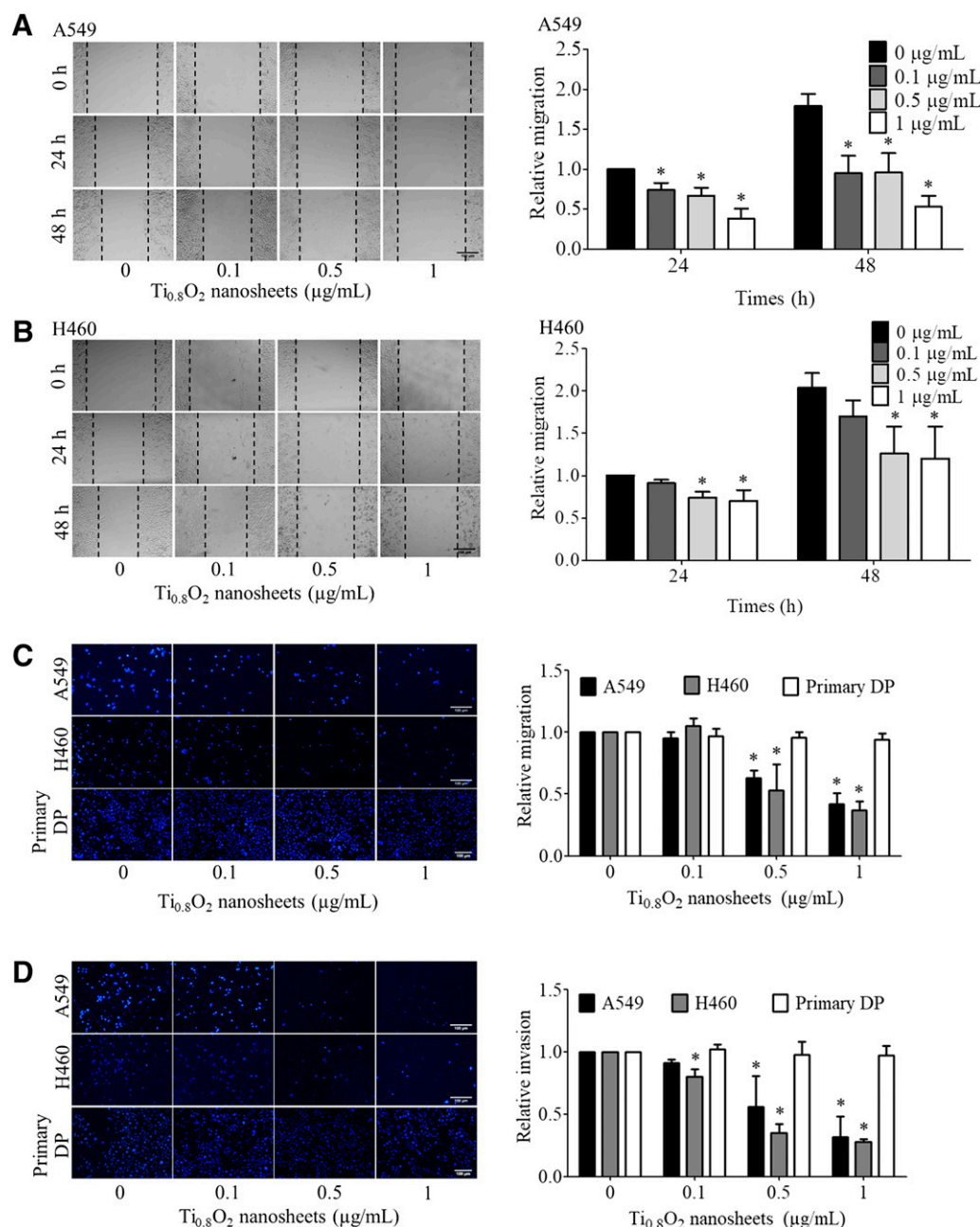


Fig. 6. Effect of Ti_{0.8}O₂ nanosheets decreases A549 and H460 cell migration and invasion. A549, H460, and primary DP1 cells were exposed to Ti_{0.8}O₂ nanosheets at concentrations of 0.1, 0.5, and 1 μg/mL, and migrations at 24 and 48 hours were investigated. The relative cell migration was determined by comparing with the control (A and B). Effect of Ti_{0.8}O₂ nanosheets on A549, H460, and primary DP1 cell migration and invasion was analyzed using Boyden chambers (8-μm pore-size filter). The relative cell migration was determined by comparing with the control (C). The relative cell invasion was investigated by comparing with the control (D). Data are shown as the mean ± S.D. (*n* = 3). **P* < 0.05 vs. nontreated control.

The human DP cell line and primary DP cells derived from different sources (primary DP1 and DP2) were cultivated in the presence of various concentrations of Ti_{0.8}O₂ nanosheets (0 to 1 μg/mL) for 72 hours and observed for aggregate formation. Figure 7 shows that Ti_{0.8}O₂ nanosheets slightly increased the sizes of cell aggregations in comparison with those of the nontreated control, in primary DP2 and DP cells, but such an induction effect did not occur in primary DP2 cells. These results indicate that treatment with Ti_{0.8}O₂ nanosheets has a minimal effect on the viability of these DP cells as well as their aggregation patterns.

Ti_{0.8}O₂ Nanosheets Selectively Target Cancer Stem Cell and EMT through Superoxide Anion-Dependent Mechanism. Having shown that Ti_{0.8}O₂ nanosheets target CSC in lung cancer cells, we searched in addition for the underlying mechanism of their CSC specificity. Intracellular ROS analysis was performed to determine the ROS generation of cancer and normal cells in response to nanosheet treatment. Figure 8 indicates that Ti_{0.8}O₂ nanosheets selectively induced the generation of intracellular superoxide anion (detected by superoxide anion specific fluorescence dye, DHE) in lung cancer cells; however, nanosheets at same concentration failed

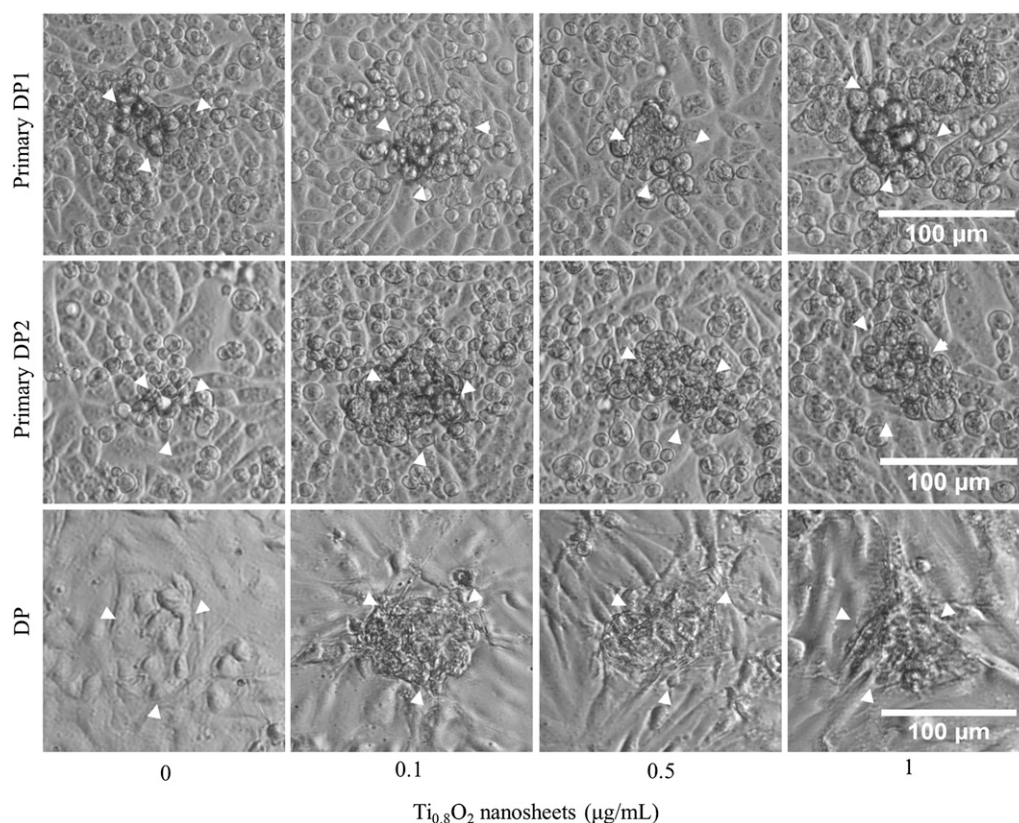


Fig. 7. Effects of $\text{Ti}_{0.8}\text{O}_2$ nanosheets on stem cell-like characteristics in primary DP cells and the DP cell line. Primary DP1, primary DP2, and DP cells were treated with $\text{Ti}_{0.8}\text{O}_2$ nanosheets (0 to 1 $\mu\text{g/ml}$) for 72 hours. Aggregation behavior of cells was determined after treatment.

to induced cellular superoxide anion (Fig. 8, A and C). For hydrogen peroxide and hydroxyl radical, both cancerous and normal DP cells responded alike (Fig. 8, A and C). We further tested whether this nanosheet-induced superoxide anion is in response to the mechanism of CSC and EMT suppression. Cells were pretreated with a specific superoxide anion inhibitor (50 μM of MnTBAP) and treated with $\text{Ti}_{0.8}\text{O}_2$ nanosheets. The cellular level of CSC and EMT markers were determined by Western blot analysis. We found that inhibition of superoxide anion in the nanosheet-treated cancer cells could restore the decrease in CSC- and EMT-related proteins (Fig. 8B). Unlike the cancer cells, treatment of the primary DP cells with MnTBAP or nanosheet cause no change in the expression of CSC and EMT markers (Fig. 8D). These results revealed that the selectivity of $\text{Ti}_{0.8}\text{O}_2$ nanosheets may be caused, at least in part, by the induction of superoxide anion in cancer cells.

Discussion

Owing to their notable properties, nanomaterials offer more effective drug delivery into cells—particularly into cancer cells—through enhanced permeability associated with nano-size (Nakamura et al., 2016). Furthermore, the use of nanoparticles in cancer cells allows retention of materials at the site of action (Nichols and Bae, 2012). Although the potential of nanoparticles to benefit delivery of drugs as well as genetic material has been intensively investigated, (Yildiz et al., 2011; Posadas et al., 2016) the understanding of unique nanoparticle shapes, especially nanosheets, and their interaction

with cancer cells are largely unknown. The shape of a nanoparticle determines the mode of cytotoxicity (Shin et al., 2015). Here, we show for the first time that $\text{Ti}_{0.8}\text{O}_2$ nanosheets distinctively suppress stem cell properties in lung CSCs but exhibit a lesser effect on noncancerous stem cells. This has been demonstrated in several lines of lung cancer in comparison with two types of primary dermal papilla and a normal keratinocyte. In addition, we have provided supportive information explaining that the cancer cell selectivity of $\text{Ti}_{0.8}\text{O}_2$ nanosheets may be caused by the generation of a superoxide anion (Fig. 8). Our results indicate that the $\text{Ti}_{0.8}\text{O}_2$ nanosheets selectively induced superoxide generation in cancer cells but not in normal DP cells (Fig. 8, A and C). The superoxide inhibition in nanosheet-treated cancer cells using a specific superoxide inhibitor further showed that the suppressing effects of $\text{Ti}_{0.8}\text{O}_2$ nanosheets on CSC and EMT were superoxide anion-dependent. Consistent with our findings, a previous study had shown that selective targeting of gold nanorods to cancer cells occurred partly through ROS generation (Wang et al., 2011).

Cancer is not a singular entity but in fact comprises multiple cell lineages with different phenotypes (Salk et al., 2010). Although unraveling and understanding the heterogeneity of the disease is at an early stage, the key player in cancer aggressiveness and relapse has been identified and named as “cancer-initiating cells” or CSCs. As a seed of the whole tumor, CSCs are unique cancer cells: They generate other cell lineages to form a tumor and they remain within the tumor and secrete several factors for support (Sengupta and Cancelas, 2010). Therefore, CSCs have become one of the

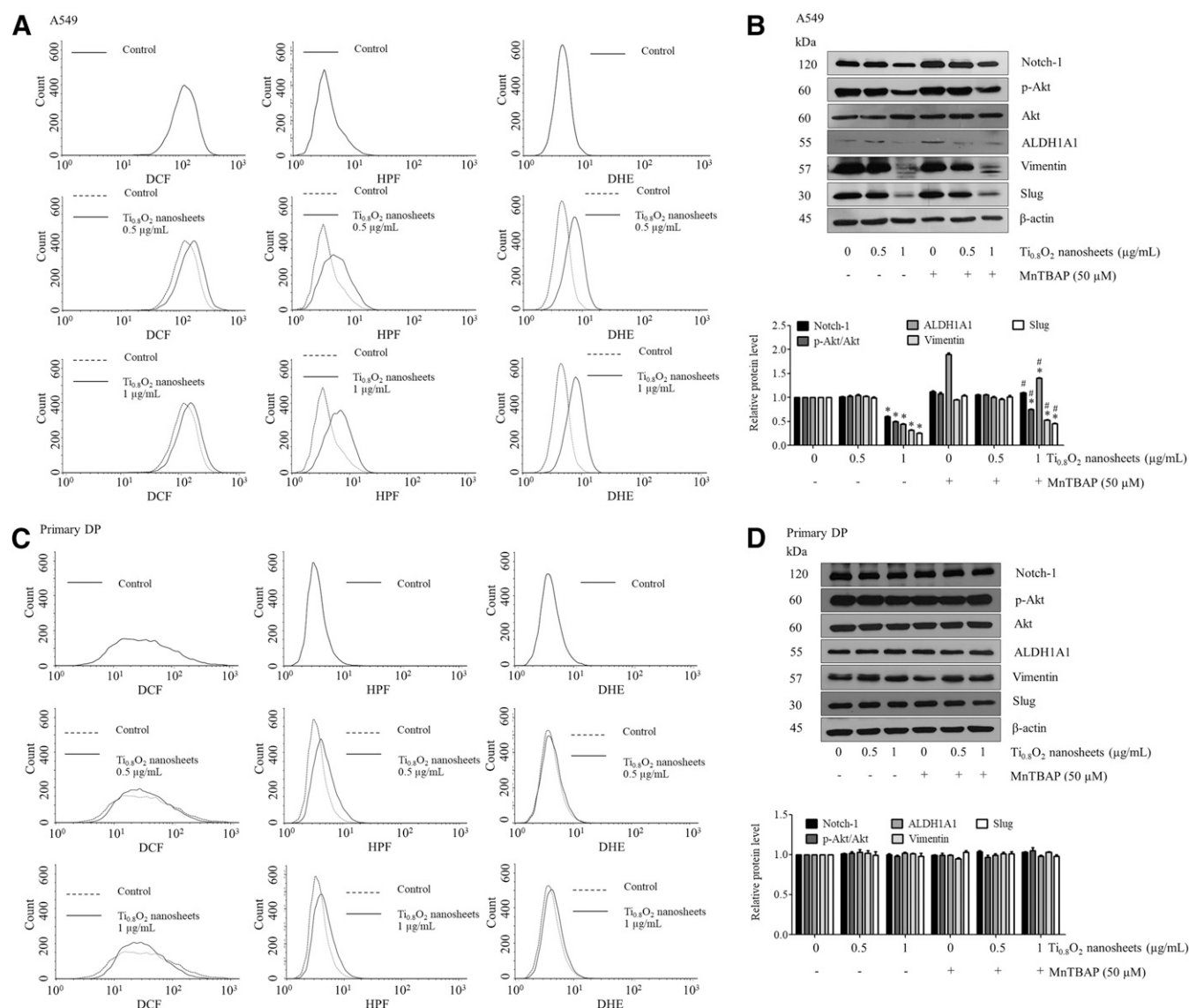


Fig. 8. TiO_2O_2 nanosheets target CSC and EMT in human lung cancer through superoxide anion. Effect of TiO_2O_2 nanosheets (0–1 $\mu\text{g/mL}$) on intracellular ROS induction at 24 hours in A549 and primary DP cells was determined by flow cytometry with fluorescent probes DCF (10 μM), HPF (10 μM), and DHE (10 μM) (A and C). Cells were treated with TiO_2O_2 nanosheets (0 to 1 $\mu\text{g/mL}$) alone for 24 hours or with the pretreatment of 50 μM MnTBAP. Protein expression levels of CSC and EMT markers were detected by Western blot analysis (B and D). Blots were reprobed with β -actin to confirm equal loading of samples. The immunoblot signals were quantified by densitometry and the mean data from independent experiments were normalized to the results. Data are shown as the mean \pm S.D. ($n = 3$). * $P < 0.05$ vs. nontreated control.

principle targets in anticancer-drug discovery in recent years (Dragu et al., 2015). The meaningful impact of CSCs in various types of cancer has increasingly been reported. Like other malignant cancers, CSCs of lung cancer have been demonstrated to be crucial for cancer initiation, progression, and metastasis (Templeton et al., 2014). Perhaps more crucially, CSCs display strong resistance to chemotherapy and later on give rise to the regrowth of the cancer cells.

Because responses to anticancer drugs can be poor, the spread of tumor cells to other sites in the patient's body and cancer relapse have been recognized as important factors accentuating the high mortality rate of lung cancer. CSC-targeted therapy and treatment strategies are urgently needed. CSCs can be recognized by their specific markers, such as ALDH1A1 and CD133, (Miyata et al., 2017) and by their cellular traits, such as colony formation

and other aggressive behaviors (Yongsanguanchai et al., 2015; Tiran et al., 2017).

Recent evidence has pointed out the role of integrins, a family of extracellular-matrix transmembrane cell-adhesion proteins, that play a part in the regulation of cancer stem cell-like phenotypes and the potential for metastasis. As solid tumors come from epithelial cells, the integrins expressed by epithelial cells are biologically retained in cancer cells, though their expression patterns and levels may be changed. Most cancerous solid-tumor cells express multiple integrins that have not only been implicated in cancer cell survival, migration and invasion, and growth but also act as receptors in interaction with the tumor stroma (Weis and Cheresh, 2011).

Certain integrins—like integrins $\beta 1$, $\beta 3$, $\alpha 5$, and αv —have been associated with poor prognosis in cancer (Rout et al., 2004). We have provided the data indicating that ouabain

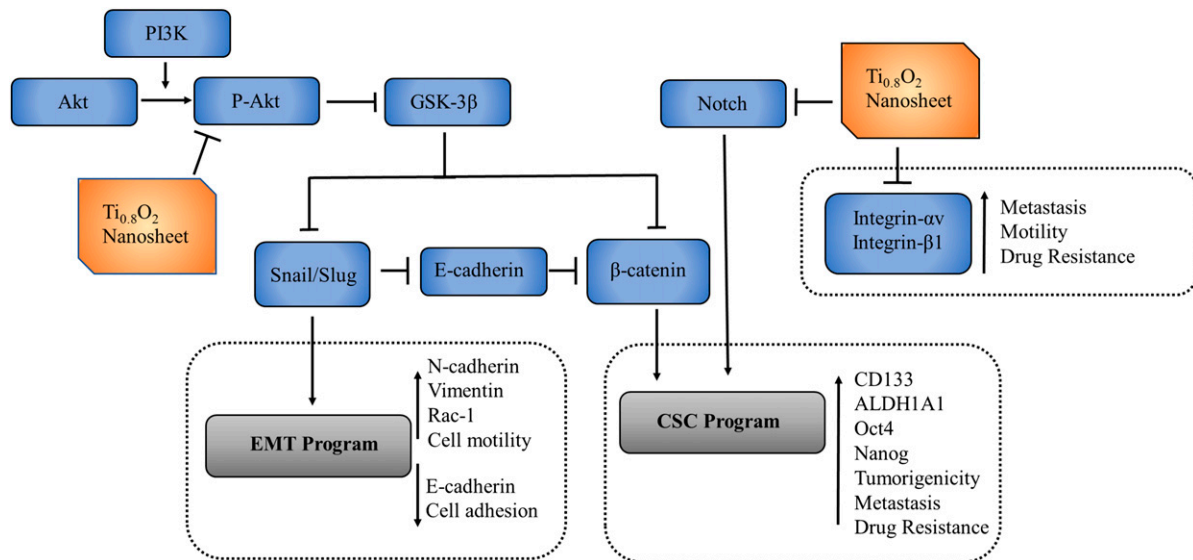


Fig. 9. Schematic diagram of $\text{Ti}_{0.8}\text{O}_2$ nanosheets suppressing CSC and EMT.

suppresses lung cancer cell migration by decreasing cellular levels of the $\alpha 4$, $\alpha 5$, $\alpha \nu$, $\beta 3$, and $\beta 4$ integrins (Ninsontia and Chanvorachote, 2014). Likewise, nitric oxide, an important biologic mediator, was shown to have no effect on the increased migratory activity of lung cancer cells via AKT-mediated upregulation of the $\alpha \nu$ and $\beta 1$ integrins (Saisongkorh et al., 2016). In lung cancer, integrin $\alpha \nu \beta 5$ has been shown to be a potential biomarker for metastasis and overall survival, and drugs targeting integrins, such as cilengitide (the $\alpha \nu \beta 3$ and $\alpha \nu \beta 5$ inhibitor), are exhibiting promising activity in phase II clinical trials. Cilengitide is currently being tested in a phase III trial in patients, so attenuating these metastasis-associated integrins could be a prospective strategy for reaching improved clinical outcomes. Our results found that treatment of lung cancer cells with $\text{Ti}_{0.8}\text{O}_2$ nanosheets suppressed the expression of integrins $\alpha \nu$ and $\beta 1$, suggesting that the additional nanosheet approach could work against cancer.

All in all, our data contributes to the emerging evidence that the $\text{Ti}_{0.8}\text{O}_2$ nanosheet exhibits very promising potential, owing to the selective role it plays in suppression of lung CSCs, with minimal cytotoxicity to normal stem cells. $\text{Ti}_{0.8}\text{O}_2$ nanosheets decreased CSC-like phenotypes and diminished the CSC markers and CSC-related transcription factors. The mechanism underlying how nanosheets decrease CSC phenotypes was found to involve the attenuation of CSC-supportive signaling such as Notch, Akt, and β -catenin. Regarding molecular mechanisms, CSCs enhance and maintain their self-renewal and differentiation activity, and CSC phenotypes, through Notch (Espinoza et al., 2013). Furthermore, Akt signaling has been shown to increase CSC phenotypes by phosphorylation at Ser9 of GSK3 β , resulting in the stabilization of the CSC regulatory protein β -catenin (Valkenburg et al., 2011). Consequently, the increased level of β -catenin confers self-renewal and tumorigenic properties on cancer cells (Valkenburg et al., 2011) (Fig. 9). Here, we have showed that $\text{Ti}_{0.8}\text{O}_2$ nanosheet treatment attenuated CSC properties in these lung cancer cells through the suppression of Akt/GSK3 β / β -catenin and Notch1, and as a consequence, the stemness of the cells was reduced. Further, nanosheets

were shown to inhibit other aggressively driven mechanisms, including the process of EMT as well as the expression of certain metastasis-associated integrins (Fig. 9). This novel finding on the role of $\text{Ti}_{0.8}\text{O}_2$ nanosheets in CSC regulation may have important implications in cancer management.

Acknowledgments

We thank the cell-based drug and health product development research unit, Faculty of Pharmaceutical Sciences, and Chulalongkorn University for their support of this study.

Authorship contributions

Participated in research design: Chanvorachote.

Conducted experiments: Petpiroon, Bhummaphan, Soonnarong, Chantarawong, Maluangnont, Pongrakhananon, Chanvorachote.

Performed data analysis: Petpiroon, Bhummaphan, Chanvorachote.

Wrote or contributed to the writing of the manuscript: Petpiroon, Bhummaphan, Maluangnont, Chanvorachote.

References

- Abell AN and Johnson GL (2014) Implications of mesenchymal cells in cancer stem cell populations: relevance to EMT. *Curr Pathobiol Rep* 2:21–26.
- Brabletz T, Lyden D, Steeg PS, and Werb Z (2013) Roadblocks to translational advances on metastasis research. *Nat Med* 19:1104–1109.
- Canel M, Serrels A, Frame MC, and Brunton VG (2013) E-cadherin-integrin crosstalk in cancer invasion and metastasis. *J Cell Sci* 126:393–401.
- Chanvorachote P and Luanpitpong S (2016) Iron induces cancer stem cells and aggressive phenotypes in human lung cancer cells. *Am J Physiol Cell Physiol* 310:C728–C739.
- Chen K, Huang YH, and Chen JL (2013) Understanding and targeting cancer stem cells: therapeutic implications and challenges. *Acta Pharmacol Sin* 34:732–740.
- De Jong WH and Borm PJA (2008) Drug delivery and nanoparticles: applications and hazards. *Int J Nanomedicine* 3:133–149.
- Dragu DL, Necula LG, Bleotu C, Diaconu CC, and Chivu-Economescu M (2015) Therapies targeting cancer stem cells: current trends and future challenges. *World J Stem Cells* 7:1185–1201.
- Espinoza I, Pochampally R, Xing F, Watabe K, and Miele L (2013) Notch signaling: targeting cancer stem cells and epithelial-to-mesenchymal transition. *Oncotargets Ther* 6:1249–1259.
- Ferlay J, Soerjomataram I, Dikshit R, Eser S, Mathers C, Rebelo M, Parkin DM, Forman D, and Bray F (2015) Cancer incidence and mortality worldwide: sources, methods and major patterns in GLOBOCAN 2012. *Int J Cancer* 136:E359–E386.
- Fukumoto S, Hsieh CM, Maemura K, Layne MD, Yet SF, Lee KH, Matsui T, Rosenzweig A, Taylor WG, Rubin JS, et al. (2001) Akt participation in the Wnt signaling pathway through Dishevelled. *J Biol Chem* 276:17479–17483.
- Gmeiner WH and Ghosh S (2015) Nanotechnology for cancer treatment. *Nanotechnol Rev* 3:111–122.
- Gravdal K, Halvorsen OJ, Haukaas SA, and Akslen LA (2007) A switch from E-cadherin to N-cadherin expression indicates epithelial to mesenchymal

- transition and is of strong and independent importance for the progress of prostate cancer. *Clin Cancer Res* **13**:7003–7011.
- Hadjimichael C, Chanoumidou K, Papadopolou N, Arampatzi P, Papamatheakis J, and Kretsovali A (2015) Common stemness regulators of embryonic and cancer stem cells. *World J Stem Cells* **7**:1150–1184.
- Jiang R, Niu X, Huang Y, and Wang X (2016) β -Catenin is important for cancer stem cell generation and tumorigenic activity in nasopharyngeal carcinoma. *Acta Biochim Biophys Sin (Shanghai)* **48**:592.
- Kadam RS, Bourne DW, and Kompella UB (2012) Nano-advantage in enhanced drug delivery with biodegradable nanoparticles: contribution of reduced clearance. *Drug Metab Dispos* **40**:1380–1388.
- Koury J, Zhong L, and Hao J (2017) Targeting signaling pathways in cancer stem cells for cancer treatment. *Stem Cells Int* **2017**:2925869.
- Kulkarni M, Mazare A, Gongadze E, Perutkova S, Kralj-Iglic V, Milošev I, Schmuki P, A Iglic, and Mozešić M (2015) Titanium nanostructures for biomedical applications. *Nanotechnology* **26**:062002.
- Laroui H, Rakhyia P, Xiao B, Vienneis E, and Merlin D (2013) Nanotechnology in diagnostics and therapeutics for gastrointestinal disorders. *Dig Liver Dis* **45**:995–1002.
- Lee JJ, Saiful Yazan L, and Che Abdullah CA (2017) A review on current nano-materials and their drug conjugate for targeted breast cancer treatment. *Int J Nanomedicine* **12**:2373–2384.
- Liu CY, Lin HH, Tang MJ, and Wang YK (2015) Vimentin contributes to epithelial-mesenchymal transition cancer cell mechanics by mediating cytoskeletal organization and focal adhesion maturation. *Oncotarget* **6**:15966–15983.
- Ma L, Zhang G, Miao XB, Deng XB, Wu Y, Liu Y, Jin ZR, Li XQ, Liu QZ, Sun DX, et al. (2013) Cancer stem-like cell properties are regulated by EGFR/AKT/ β -catenin signaling and preferentially inhibited by gefitinib in nasopharyngeal carcinoma. *FEBS J* **280**:2027–2041.
- Maluangnont T, Arsa P, Limsakul K, Juntarachairot S, Sangsan S, Gotoh K, and Sooknoi T (2016) Surface and interlayer base-characters in lepidocrocite titanate: the adsorption and intercalation of fatty acid. *J Solid State Chem* **238**:175–181.
- Maluangnont T, Chanlek N, Suksawad T, Tonket N, Saikhamee P, Sukkha U, and Vittayakorn N (2017) Beyond soft chemistry - bulk and surface modifications of polycrystalline lepidocrocite titanate induced by post-synthesis thermal treatment. *Dalton Trans* **46**:14277–14285.
- Maluangnont T, Matsuba K, Geng F, Ma R, Yamauchi T, and Sasaki T (2013) Osmotic swelling of layered compounds as a route to producing high-quality two-dimensional materials. A comparative study of tetramethylammonium versus tetrabutylammonium cation in a lepidocrocite-type titanate. *Chem Mater* **25**:3137–3146.
- Medici D, Hay ED, and Olsen BR (2008) Snail and Slug promote epithelial-mesenchymal transition through β -catenin-T-cell factor-4-dependent expression of transforming growth factor- β 3. *Mol Biol Cell* **19**:4875–4887.
- Miyata T, Oyama T, Yoshimatsu T, Higa H, Kawano D, Sekimura A, Yamashita N, So T, and Gotoh A (2017) The clinical significance of cancer stem cell markers ALDH1A1 and CD133 in lung adenocarcinoma. *Anticancer Res* **37**:2541–2547.
- Mohammed MK, Shao C, Wang J, Wei Q, Wang X, Collier Z, Tang S, Liu H, Zhang F, Huang J, et al. (2016) Wnt/ β -catenin signaling plays an ever-expanding role in stem cell self-renewal, tumorigenesis and cancer chemoresistance. *Genes Dis* **3**:11–40.
- Molina JR, Yang P, Cassivi SD, Schild SE, and Adjei AA (2008) Non-small cell lung cancer: epidemiology, risk factors, treatment, and survivorship. *Mayo Clin Proc* **83**:584–594.
- Nakamura Y, Mochida A, Choyke PL, and Kobayashi H (2016) Nanodrug delivery: is the enhanced permeability and retention effect sufficient for curing cancer? *Bioconjug Chem* **27**:2225–2238.
- Neelakantan D, Drasin DJ, and Ford HL (2015) Intratumoral heterogeneity: clonal cooperation in epithelial-to-mesenchymal transition and metastasis. *Cell Adhes Migr* **9**:265–276.
- Nichols JW and Bae YH (2012) Odyssey of a cancer nanoparticle: from injection site to site of action. *Nano Today* **7**:606–618.
- Ninsontia C and Chanvorachote P (2014) Ouabain mediates integrin switch in human lung cancer cells. *Anticancer Res* **34**:5495–5502.
- Nune SK, Gunda P, Thallapally PK, Lin YY, Forrest ML, and Berkland CJ (2009) Nanoparticles for biomedical imaging. *Expert Opin Drug Deliv* **6**:1175–1194.
- Phiboonchaiyanan PP, Kiratipaiboon C, and Chanvorachote P (2016) Ciprofloxacin mediates cancer stem cell phenotypes in lung cancer cells through caveolin-1-dependent mechanism. *Chem Biol Interact* **250**:1–11.
- Posadas I, Monteagudo S, and Ceña V (2016) Nanoparticles for brain-specific drug and genetic material delivery, imaging and diagnosis. *Nanomedicine (Lond)* **11**:833–849.
- Powan P, Luanpitpong S, He X, Rojanasakul Y, and Chanvorachote P (2017) Detachment-induced E-cadherin expression promotes 3D tumor spheroid formation but inhibits tumor formation and metastasis of lung cancer cells. *Am J Physiol Cell Physiol* **313**:C556–C566.
- Rout UK, Wang J, Paria BC, and Armand DR (2004) $\alpha 5 \beta 1$, $\alpha v \beta 3$ and the platelet-associated integrin $\alpha IIb \beta 3$ coordinately regulate adhesion and migration of differentiating mouse trophoblast cells. *Dev Biol* **268**:135–151.
- Saisongkroh V, Maiuthed A, and Chanvorachote P (2016) Nitric oxide increases the migratory activity of non-small cell lung cancer cells via AKT-mediated integrin αv and $\beta 1$ upregulation. *Cell Oncol (Dordr)* **39**:449–462.
- Salk JJ, Fox EJ, and Loeb LA (2010) Mutational heterogeneity in human cancers: origin and consequences. *Annu Rev Pathol* **5**:51–75.
- Sari AR, Rufaut NW, Jones LN, and Sinclair RD (2016) Characterization of ovine dermal papilla cell aggregation. *Int J Trichology* **8**:121–129.
- Sasaki T and Watanabe M (1998) Osmotic swelling to exfoliation. exceptionally high degrees of hydration of a layered titanate. *J Am Chem Soc* **120**:4682–4689.
- Sasaki T and Watanabe M (1997) Semiconductor nanosheet crystallites of quasi-TiO₂ and their optical properties. *J Phys Chem B* **101**:10159–10161.
- Sengupta A and Cancelas JA (2010) Cancer stem cells: a stride towards cancer cure? *J Cell Physiol* **225**:7–14.
- Shin SW, Song IH, and Um SH (2015) Role of physicochemical properties in nanoparticle toxicity. *Nanomaterials (Basel)* **5**:1351–1365.
- Slifka MK and Ahmed R (1996) Limiting dilution analysis of virus-specific memory B cells by an ELISPOT assay. *J Immunol Methods* **199**:37–46.
- Song S-S, Xia B-Y, Chen J, Yang J, Shen X, Fan S-J, Guo M-L, Sun Y-M, and Zhang X-D (2014) Two dimensional TiO₂ nanosheets: in vivo toxicity investigation. *RSC Advances* **4**:42598–42603.
- Templeton AK, Miyamoto S, Babu A, Munshi A, and Ramesh R (2014) Cancer stem cells: progress and challenges in lung cancer. *Stem Cell Investig* **1**:9.
- Tiran V, Lindenmann J, Bric L, Heitzer E, Stanzer S, Tabrizi-Wizsy NG, Stacher E, Stoeger H, Popper HH, Balic M, et al. (2017) Primary patient-derived lung adenocarcinoma cell culture challenges the association of cancer stem cells with epithelial-to-mesenchymal transition. *Sci Rep* **7**:10040.
- Tomisa AP, Launey ME, Lee JS, Mankani MH, Wegst UGK, and Saiz E (2011) Nanotechnology approaches to improve dental implants. *Int J Oral Maxillofac Implants* **26** (Suppl):25–44, discussion 45–49.
- Valkenburg KC, Graveel CR, Zylstra-Diegel CR, Zhong Z, and Williams BO (2011) Wnt/ β -catenin signaling in normal and cancer stem cells. *Cancers* **3**:2050–2079.
- Wang D, Plukker JTM, and Coppes RP (2017) Cancer stem cells with increased metastatic potential as a therapeutic target for esophageal cancer. *Semin Cancer Biol* **44**:60–66.
- Wang L, Liu Y, Li W, Jiang X, Ji Y, Wu X, Xu L, Qiu Y, Zhao K, Wei T, et al. (2011) Selective targeting of gold nanorods at the mitochondria of cancer cells: implications for cancer therapy. *Nano Lett* **11**:772–780.
- Wang L and Sasaki T (2014) Titanium oxide nanosheets: graphene analogues with versatile functionalities. *Chem Rev* **114**:9455–9486.
- Weis SM and Chersesh DA (2011) αv integrins in angiogenesis and cancer. *Cold Spring Harb Perspect Med* **1**:a006478.
- Xia P and Xu XY (2015) PI3K/Akt/mTOR signaling pathway in cancer stem cells: from basic research to clinical application. *Am J Cancer Res* **5**:1602–1609.
- Yildiz I, Shukla S, and Steinmetz NF (2011) Applications of viral nanoparticles in medicine. *Curr Opin Biotechnol* **22**:901–908.
- Yin ZF, Wu L, Yang HG, and Su YH (2013) Recent progress in biomedical applications of titanium dioxide. *Phys Chem Chem Phys* **15**:4844–4858.
- Yongsanguanchai N, Pongrakhananon V, Mutirangura A, Rojanasakul Y, and Chanvorachote P (2015) Nitric oxide induces cancer stem cell-like phenotypes in human lung cancer cells. *Am J Physiol Cell Physiol* **308**:C89–C100.
- Zhao J (2016) Cancer stem cells and chemoresistance: the smartest survives the raid. *Pharmacol Ther* **160**:145–158.

Address correspondence to: Dr. Pithi Chanvorachote, Department of Pharmacology and Physiology, Faculty of Pharmaceutical Sciences, and Cell-based Drug and Health Product Development Research Unit, Chulalongkorn University, Bangkok 10330, Thailand. E-mail: pithi_chan@yahoo.com